

The central role of oxo clusters in zirconium- and hafnium-based esterification catalysis

Jikson Pulparayil Mathew,[†] Carlotta Seno,[†] Mohit Jaiswal,[‡] Charlotte Simms,[¶]
Nico Reichholf,[†] Dietger Van den Eynden,[†] Tatjana N. Parac-Vogt,[¶] and
Jonathan De Roo^{*,†}

[†]*Department of Chemistry, University of Basel, Mattenstrasse 22, 4058 Basel, Switzerland*

[‡]*Department of Chemical Sciences, Indian Institute of Science Education and Research (IISER)-Mohali, Mohali, SAS Nagar, Punjab, 140306, India*

[¶]*Department of Chemistry, KU Leuven, Celestijnenlaan 200F, 3001 Leuven, Belgium*

E-mail: Jonathan.DeRoo@unibas.ch

Abstract

Oxo clusters are a unique link between oxide nanocrystals and MOFs, representing the limit of downscaling each of the respective crystals. Here, we show the superior catalytic activity of $\text{Zr}_{12}\text{O}_8(\text{OH})_8(\text{OOCR})_{24}$ clusters, compared to zirconium MOF UiO-66 and ZrO_2 nanocrystals. We focus on esterification reactions given their general importance in consumer products and the challenge of converting large substrates. Oxo clusters have a higher surface-to-volume ratio than nanocrystals, rendering them more active. For large substrates, e.g., oleic acid, MOF UiO-66 has negligible catalytic activity while clusters provide almost quantitative conversion, a fact we ascribe to limited diffusion of large substrates through the MOF pores. Cluster do not suffer from limited mass transfer and we also obtain high conversion in solvent-free reactions with sterically hindered alcohols (hexanol, 2-ethylhexanol, benzyl alcohol and neopentyl

alcohol). The cluster catalyst can be recovered and shows identical activity. The structural integrity of the cluster is confirmed using X-ray total scattering and Pair Distribution Function analysis. Even more, when homogeneous zirconium (or hafnium) alkoxides are used as catalyst, the same oxo cluster is retrieved, showing that oxo clusters are the active catalytic species, even in previously assumed homogeneously catalyzed reactions.

Introduction

Homogenous and heterogeneous catalyst materials are, in principle, two distinct and well-defined groups, being either the same phase as the substrate or different. Homogeneous catalysts are metal salts or metal complexes that dissolve in the reaction medium and are most often not recovered. Heterogeneous catalysts are often insoluble powders, dispersed in the reaction medium through stirring, and the powder is easily recovered by filtration. Typical examples of heterogeneous catalysts are (i) bulk oxide or (ii) Metal Organic Frameworks (MOFs). With the advent of nanocrystal synthesis,¹ an opportunity was created to make heterogeneous catalysts more active by increasing their surface area or exposing certain facets.²⁻⁴ While aggregated or supported nanocrystals still appear as a powder, colloidal nanocrystals (of only a few nanometer in size) form stable solutions without any light scattering. One can debate whether colloidal nanocrystals belong to the realm of homogeneous or heterogeneous catalysis. They feature a solid-liquid interface but are homogeneously dispersed in solution. To further muddle the definitions, there are claims that certain homogeneous catalyst forms colloidal nanocrystals during catalysis.⁵

When further increasing the surface-to-volume ratio of nanocrystals by decreasing their size, one reaches a limit, beyond which, the material would lose its particle character and become a metal complex. For example, in the case of zirconia, we can conceive a spheroidal particle containing 6 zirconium atoms where the atomic arrangement of zirconium and oxygen is still identical to the one in the cubic crystal structure of zirconia. The surface is capped

with (carboxylate) ligands, just like for colloidal nanocrystals. Such objects are known as discrete oxo clusters.^{6,7} Exactly the same structure is obtained when scaling down zirconium MOF (nano)crystals until only a single secondary building unit is left with monofunctional ligands instead of bifunctional linkers. Discrete oxo clusters thus provide the missing link between oxide nanocrystals and MOFs and their relationship is illustrated in Figure 1. This link is the object of our study.

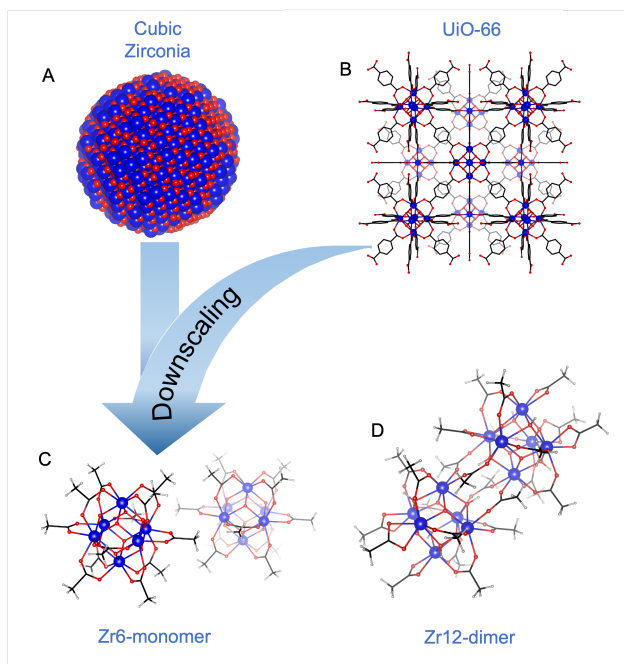


Figure 1: Structural representation of catalysts used in this paper. (A) Nanocrystal (ZrO_2), (B) Metal-Organic Framework (UiO-66),⁸ (C) **Zr6** oxo cluster (**Zr6**-acetate),⁹ and (D) **Zr12** oxo cluster (**Zr12**-acetate)

So far, nanocrystals and MOFs have been extensively researched in the field of catalysis. Nanocrystals are currently exploited in thermal catalysis,^{10–12} electrochemical reactions^{13–15} and photochemical processes.^{16–18} MOFs are developed as heterogeneous catalysts.^{19–27} Their high porosity and high surface area made MOFs highly appealing, either as support or as an intrinsic catalyst.²⁸ In the latter case, the metal atoms in the nodes are the catalytic centers. The steric and electronic properties of the linkers can be engineered to influence the activity of the metal node.^{29–31} Within the group 4 MOFs, the nodes are metal oxo clusters. Group 4 MOFs have been extensively researched due to their high stability, Lewis

acidity, and tunable structure.^{32,33} To improve their catalytic activity, defects are often introduced.³⁴ These MOFs have been employed in hydrolysis reactions,^{35,36} esterification,^{37,38} amide bond formation,³⁹ cyclization reaction,⁴⁰ asymmetric deacetalization - acetalization reactions,⁴¹ enantioselective Friedel–Crafts Reaction,⁴¹ and condensation reaction.^{42,43} However, the catalytic activity of MOFs seems to be poor towards large and bulky substrates, for which diffusion through the small pores becomes very slow.^{44–46} Research has therefore focused on designing MOFs with larger pore sizes or with smaller crystallite sizes to increase the active surface area and minimise the effect of internal diffusion on reaction kinetics.^{46–50}

To maximize the number of active sites, we and others recently started exploring soluble zirconium and hafnium oxo clusters as homogeneous catalysts. These clusters have a M_6O_8 core, capped with protons and carboxylates. The clusters typically appear either as monomers ($Zr_6O_4(OH)_4(OOCR)_{12}$), or as dimers ($Zr_{12}O_8(OH)_8(OOCR)_{24}$), depending on the steric hindrance of the carboxylate ligand.^{6,51} Even though polyoxometalates anions have been widely reported in the field of catalysis,^{52–54} neutral oxo clusters are less explored. Zirconium oxo clusters were used for amide bond formation,^{7,55} amine oxidation,⁵⁶ hydrogen peroxide activation,⁵⁷ and proteolysis.⁵⁸ In addition, oxo clusters are atomically precise objects (in contrast to MOFs or nanocrystals) and thus open exciting opportunities for mechanistic studies.

Here, we propose zirconium and hafnium oxo clusters as highly active catalysts for the esterification of bulky acid or alcohol substrates. Their esters are relevant as biofuels, emollients, plasticizers, and lubricants.^{59–63} Oxo clusters are by far superior catalysts compared to oxide nanocrystals and MOFs due to their maximal surface-to-volume and the absence of diffusion limitations. We further showed that the oxo cluster structure is stable during catalysis, aided by X-ray total scattering and Pair Distribution Function (PDF) Analysis. Even more, we find that oxo clusters are formed when metal alkoxides are employed as pre-catalysts, thus elucidating the active species in previously reported catalytic reactions.

Results and discussion

Superior catalytic activity of oxo clusters

To demonstrate the superior catalytic activity of zirconium oxo clusters with respect to zirconium MOFs and ZrO₂ nanocrystals, we choose esterification as a model reaction due to its wide application in the pharmaceutical⁶⁴ and cosmetic industry.⁶⁵ Esterification is also used for the production of emulsifiers,^{66,67} plasticizers,⁶⁸ and biodiesel.^{69–72} UiO-66, ZrO₂ nanocrystals, and **Zr12** oxo clusters were synthesised according to previously published procedures.^{51,73–75} Oleate was chosen as the ligand for the oxo clusters and nanocrystals since oleic acid is the first substrate for our chosen catalytic reaction, thus avoiding competition between ligand and catalytic substrate for the surface binding sites, and avoiding the production of unwanted side-products.⁷⁶ The ZrO₂ nanocrystals, synthesized from zirconium isopropoxide and benzyl alcohol, have an average diameter of 5.6 nm, see Figure S1. The ¹H NMR spectrum shows only broadened resonances of bound oleate ligands (Figure S2).^{77,78} UiO-66 was synthesized from ZrCl₄ and benzene-1,4-dicarboxylic acid and dried in air at 70 °C for 4 h and then activated at 110 °C for 20 h to remove residual solvent from the pores. The synthesised MOF was analysed via pXRD (Figure S5) to confirm the crystallinity of the material and was also digested in NaOH and analyzed by ¹H NMR (Figure S6) to determine the linker connectivity of UiO-66. The inorganic fraction was determined using TGA (Figure S7) and together with ¹H NMR revealed the presence of approximately 1 missing linker per cluster. Quantifying the number of open metal sites is important for catalysis as the substrate (oleate) must bind to the Zr for the reaction to proceed. This stands in contrast to nanocrystals and oxo clusters where oleate was directly bound to Zr as the stabilising ligand. The oleate-capped oxo cluster (**Zr12**-oleate), synthesised from zirconium propoxide and oleic acid, is a dimer of two **Zr6** octahedral clusters (PDF in Figure S3 and NMR in Figure S4). The activity of all three catalysts were evaluated in the esterification of oleic acid with ethanol as a model reaction (Figure 2). 1 mol% of **Zr12** cluster was added to the

reaction mixture, amounting to 12 mol% zirconium. Equal amounts of zirconium (12 mol%) were present in the nanocrystal and MOF catalysts. After 12 hours of reaction, almost full conversion was obtained when using the cluster as the catalyst, while the ZrO_2 nanocrystals only featured a slightly higher conversion compared to the reaction without a catalyst. Interestingly, UiO-66 does not show any appreciable catalytic activity.

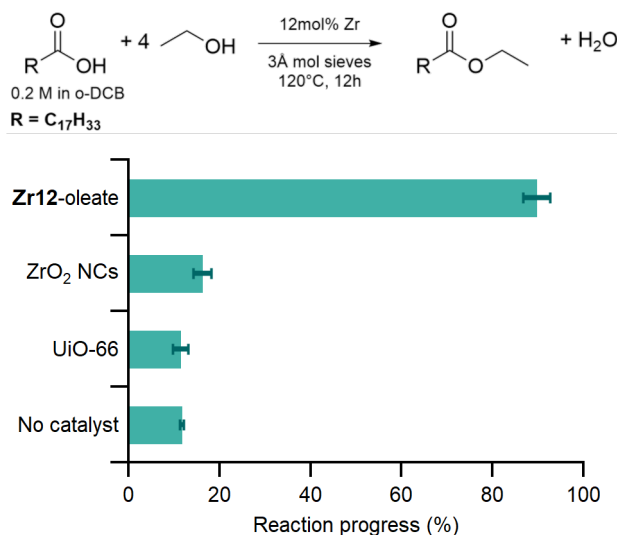


Figure 2: Catalytic esterification of oleic acid with ethanol in ortho-dichlorobenzene (o-DCB). The catalyst is either **Zr12**-oleate, ZrO_2 nanocrystals or the MOF UiO-66. The reactions were performed in triplicate

The striking difference between nanocrystals and clusters can be partly ascribed to a difference in surface area. In the **Zr12**-oleate cluster, all zirconium atoms are available at the surface, thus presenting a maximal surface area of around 77 \AA^2 per octahedron (calculated by approximating it to a sphere). In 5.6 nm nanocrystals, about 80% of the zirconium atoms are buried beneath the surface.⁵¹ If the difference in activity was only due to a different number of catalytic sites, the turnover number (TON, calculation in the SI) for nanocrystals and clusters would be the same, when calculated per surface metal site. However, after subtracting the control from the reaction progress, the TON was 1.9 and 6.5 for nanocrystals and clusters respectively (see the SI for the calculations). This means that the clusters are also intrinsically more catalytically active. The steric factor could play a role

since clusters have a higher surface curvature than nanocrystals and thus ligands are more densely packed on nanocrystals, hampering the approach of the alcohol. The curvature of a sphere is given by the reciprocal of radius; we calculate a curvature of 0.4 Å and 0.036 Å for cluster and nanocrystal respectively. In addition, clusters can act as both hydrogen bond donors and acceptors since their surface has μ_3 oxygen atoms with and without attached hydrogen atoms.⁶ This makes them ideally suited to activate the alcohol.

The difference in the catalytic activity between MOFs and clusters can be ascribed to node accessibility. In MOFs, diffusion of the large substrate through the pores is slow and catalysis likely only happens at the surface of the MOF microcrystals. To verify this hypothesis, we explored the substrate scope; using acetic acid, butanoic acid, and oleic acid as substrates. As clusters catalysts, we used **Zr12**-acetate, **Zr12**-butanoate, and **Zr12**-oleate respectively, to avoid competition between ligand and the incoming substrate.⁷⁶ The reaction was monitored for 3 hours by taking an aliquot at a time interval of 1 hour, see Figure 3. For carboxylic acids with longer chain lengths, the reaction progress decreased for all catalysts. However, the reactivity decreased more drastically for the MOF catalyst. While the ethyl acetate yield is considerably higher than the control (without catalyst), this is less so for ethyl butanoate. For ethyl oleate, the conversion using MOFs is equal to the reaction without a catalyst. Therefore, we conclude that the UiO-66 MOF is a suitable esterification catalyst for small substrates but clusters are superior catalysts for bulky substrates.

To get a deeper insight into the catalytic activity of oxo clusters, we explored the influence of various parameters, see Table 1. Entry **(1)** represents the 12 hour reaction as in Figure 1 while the other entries are recorded after 3 hours of reaction. As expected, with increasing equivalents of ethanol, higher yields are obtained, see Entries **(2)**-**(5)** (and Figure S8). The addition of 3 Å molecular sieves had also a positive effect (Entries **(3)** and **(6)** (and Figure S9)), since they could help in the removal of water, formed as a side product during the esterification, pushing the equilibrium to the right. Replacing ortho-dichlorobenzene (o-DCB) with mesitylene does not affect the yield (Entries **(3)** and **(7)**).

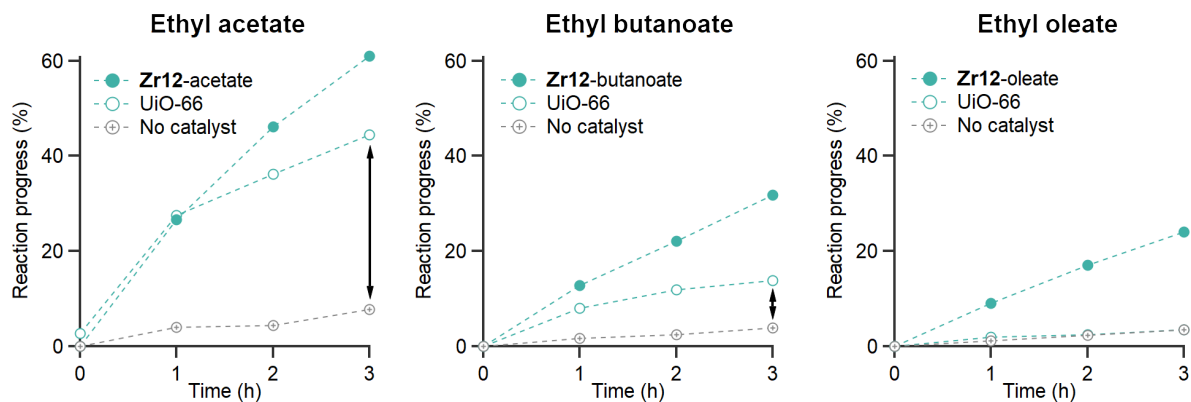


Figure 3: Catalytic esterification, comparing **Zr12** oxo clusters and UiO-66, for different carboxylic acid substrates. The conditions are identical to Figure 1: 120 °C, 12 mol% zirconium, 0.2M carboxylic acid, molecular sieves, and 4 equivalents of ethanol.

Table 1: The esterification of oleic acid with ethanol, using **Zr12**-oleate as the catalyst. The catalyst amount is always 1 mol% dimer compared to the total substrate (oleic acid + oleate), which is equivalent to 12mol% Zr.

Entry	Alcohol equiv	Solvent	Sieves	Temp.	Time	Yield
(1)	4	o-DCB	Yes	120 °C	12 hr	89.6%
(2)	2	o-DCB	Yes	120 °C	3 hr	17%
(3)	4	o-DCB	Yes	120 °C	3 hr	27%
(4)	6	o-DCB	Yes	120 °C	3 hr	37%
(5)	10	o-DCB	Yes	120 °C	3 hr	45%
(6)	4	o-DCB	No	120 °C	3 hr	18%
(7)	4	Mesitylene	Yes	120 °C	3 hr	28%

Solventless esterification using higher alcohols

Since reactions without an additional solvent are highly desirable and more sustainable, we explored solventless reactions with high-boiling alcohols. The latter are also generally more challenging and less reactive than ethanol or methanol. In case of hexanol, we compared

the standard reaction (using 4 equivalents of hexanol) in mesitylene with a reaction where the solvent was omitted, and another reaction where the amount of hexanol was reduced to 1.2 equivalents. Given that the total volume of the latter reaction mixture decreases, the concentration of carboxylic acid and catalyst increases. While a moderate conversion was observed after only 3 hours in mesitylene, 69% yield was obtained in the solvent-free reaction (Figure 4). The catalyzed yield decreased to 61% for only 1.2 equivalents of hexanol while the yield without catalyst increased slightly to 28%. The reaction with 1.2 equivalents of hexanol does have the highest atom economy and is for that reason interesting. Note that the yield was calculated assuming that the oleate ligand on the cluster also acts as a substrate. If one excludes the oleate ligands on the catalyst, the yield is adjusted from 61% to 80% for the reaction with 1.2 equivalents of hexanol. This point is further reinforced by the fact that the recovered cluster catalyst contains oleate ligands on its surface (*vide infra*), suggesting that the oleate ligand is not substrate.

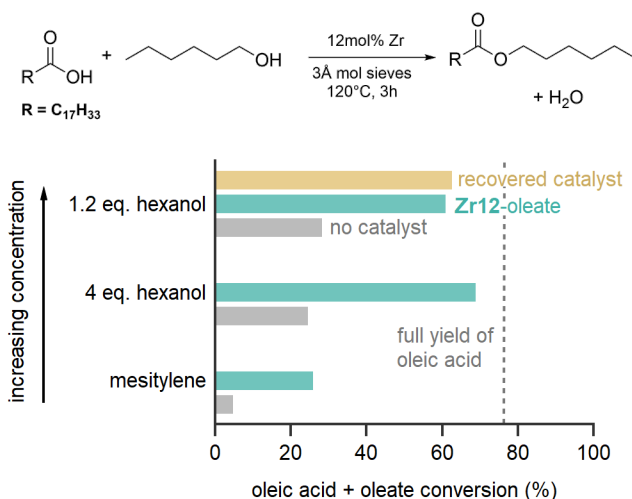
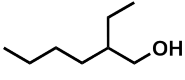
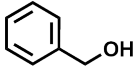
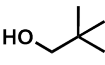
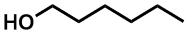


Figure 4: Catalytic esterification of oleic acid with hexanol. The reaction is either done in mesitylene (using 4 equivalents hexanol), without mesitylene (using 4 equivalents hexanol), or without mesitylene and a reduced 1.2 equivalents of hexanol. In the latter case, we recovered the catalyst and used this for a second catalytic reaction.

The substrate scope of the oxo cluster catalyst was further explored using sterically hindered alcohols such as 2-ethylhexanol, benzyl alcohol, and neopentyl alcohol (Table 2)

as substrates. While benzyl alcohol converts readily, giving a similar yield to hexanol, 2-ethylhexanol and neopentyl alcohol give lower yield but still an appreciable conversion. Finally, hafnium oxo clusters exhibit a yield of 57% for the formation of hexyloleate ester, similar to that of zirconium oxo clusters (61%)(Figure S10).

Table 2: Catalytic esterification of oleic acid with 1.2 equivalents of alcohols, using **Zr12**-oleate as the catalyst. The catalyst amount is 1 mol% dimer compared to the acid substrate (5 mmol), which is equivalent to 12 mol% Zr. The reaction is conducted at 120 °C with molecular sieves for 3 or 6 hours.

Entry	Alcohol	Yield	Control		
			3h	6h	
(1)		51%	25%	71%	42%
(2)		65%	19%	85%	32%
(3)		43%	23%	65%	37%
(4)		68%	28%	83%	43%

Mechanistic insight in the active species

Although the clusters are homogeneously dissolved in the reaction mixture, they were recovered after the reaction by precipitation with acetonitrile followed by washing with acetone. Taking the solvent-free esterification of oleic acid with 1.2 equivalents hexanol as a representative reaction (with 61% yield), the catalyst was recovered and used again in a second reaction (Figure 4). The activity remained the same, suggesting that the catalyst is stable. As shown by thermogravimetric analysis (TGA), the recovered cluster has the same inorganic content as the as-synthesized cluster (Figure S11). Also the NMR and IR spectra before and after catalysis are similar (Figure S12 and S13). To gain more precise insight into the structure of the cluster core, we turned to Pair Distribution Function (PDF) analysis.⁵¹ Figure 5 shows the PDF of the as-synthesized clusters, and the recovered clusters after

the first and second catalytic reaction. The patterns are remarkably alike indicating that the overall Zr_6O_8 cluster structure is retained. However, the dimeric nature of the cluster changes. Before catalysis, the clusters are best described by the dimer structure, while after reaction, a better refinement was obtained for a monomeric cluster structure (Figure S14). A dual-phase refinement was performed combining **Zr6**- and **Zr12**-propionate structure models,⁷⁹ giving a better fit and providing the ratio between monomer and dimer (Figure 5). This analysis indicated that the structure of the cluster before catalysis was composed of 59% **Zr12** dimer and 41% of **Zr6**. However, after catalysis, the ratio of monomer increases from 41% to 73% after the first cycle and 74% after the second. Most importantly, it can be concluded that the Zr_6O_8 cluster core remains intact and acts as the catalytically active species.

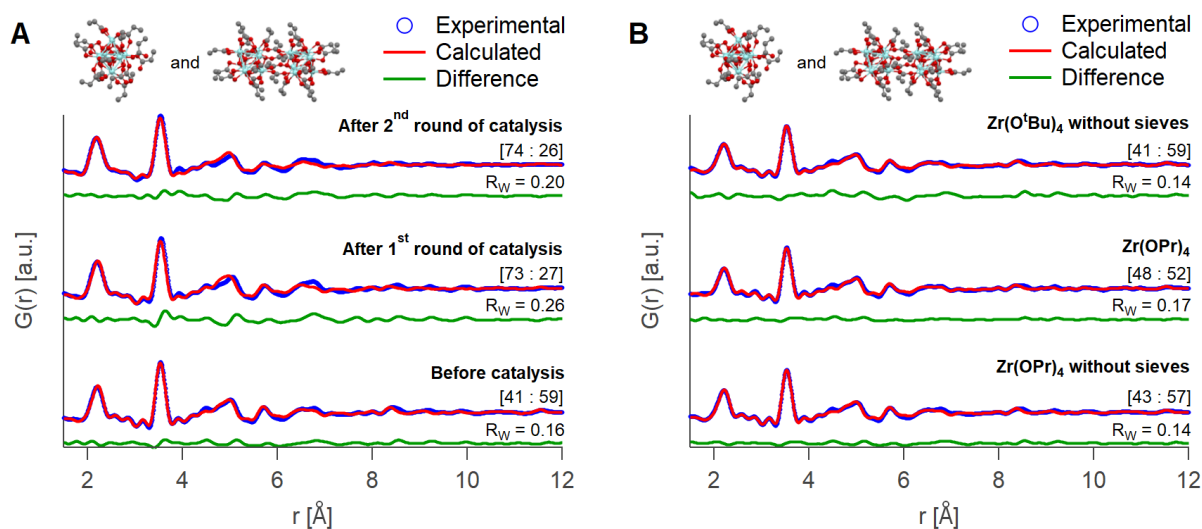


Figure 5: PDF refinement for (A) **Zr12**-oleate cluster before catalysis, and after the first and second round of catalysis, (B) and for catalyst recovered at different time intervals with and without molecular sieves after using $Zr(OPr)_4$ as the catalyst. The values in square brackets correspond to the ratio of monomer to dimer cluster in the fit. The refinement is performed using both **Zr6**- and **Zr12**-propionate structure obtained from the single crystal structure of $[Zr_6O_4(OH)_4(OOCR)_{12}]_2$ (CCDC 604529).⁷⁹ The refined parameters are indicated in Figures S16 and S17.

The above structural conclusions were drawn for reactions where the overall conversion

(oleic acid + oleate ligand) does not exceed 76%. Above this conversion, the oleate ligands of the cluster catalyst are converted into ester, which leads to a structural rearrangement or deterioration of the cluster. For example, for a reaction where the conversion was 94%, the cluster structure is severely compromised as indicated by PDF analysis (Figure S18). When the overall conversion is only slightly above 76%, (e.g., 78%) the Zr_6O_8 cluster structure is still identified in PDF although some structural changes are already present (see Figure S18).

The active species in homogeneous catalysis

Zirconium alkoxides were previously employed as homogenous catalysts.⁸⁰ We hypothesized that such homogenous compounds are simply pre-catalysts and that they form the **Zr6** clusters *in situ*. Indeed, we isolated oxo clusters from the esterification reaction of oleic acid by 1.2 equiv hexanol using 12 mol% of $\text{Zr}(\text{OPr})_4$ or $\text{Zr}(\text{O}^t\text{Bu})_4$ (comparable conditions to Table 2). The NMR spectra (Figure S20, S21 and S22) are consistent with oleate capped clusters and PDF refinements further confirm the structure of the inorganic cluster core (Figure 5B). The absence or presence of molecular sieves does not change the cluster structure. It is not too surprising that clusters are formed under esterification conditions since esterification is used for cluster synthesis.⁵¹ As a final note, $\text{Zr}(\text{O}^t\text{Bu})_4$ yielded 63% hexyloleate ester after 3h, similar to the yield from cluster catalysts. For $\text{Zr}(\text{OPr})_4$ the total ester yield was 78%. However, propyl ester was also observed as a side-product (Figure S19) due to the higher reactivity of propanol to hexanol. Tert-butanol does not show any reactivity and does not produce side-products.

Conclusion

Discrete clusters have superior catalytic activity compared to MOFs and oxide nanocrystals. While oxide nanocrystals have a lower surface area than clusters, MOFs with small pores

hamper diffusion, especially for large substrates. Using cluster catalysts, we demonstrated high yields for the esterification of oleic acid with sterically hindered alcohols, in solventless conditions. Through structural studies, aided by X-ray total scattering and PDF analysis, we confirmed that the oxo clusters are stable during catalysis. The cluster catalysts can be recovered without altering their basic structure or activity. Furthermore, we showed that several homogeneous zirconium and hafnium catalysts transform into oxo clusters during the reaction, thus assigning oxo clusters as the catalytically active species.

Experimental

Materials. Zirconium propoxide (70w% in 1-propanol), hafnium butoxide (99%), butyric acid ($\geq 90\%$), 1,2-Dichlorobenzene (99%, anhydrous) and Mesitylene (98%) were provided by Sigma Aldrich and these were stored in a Straus flask upon arrival. Acetic acid ($>99\%$) was purchased from Sigma Aldrich, vacuum transferred, and stored in a Straus flask. Zirconium isopropoxide and zirconium tertbutoxide were synthesized in the Lab.⁸¹ Oleic acid ($>99\%$, GC) was bought from TCI chemicals. For cluster synthesis, oleic acid (90%, technical grade) from Sigma Aldrich was used. Benzyl alcohol (anhydrous, 99.8%), 2,2-Dimethyl-1-propanol (99%), and 2-Ethyl-1-hexanol ($\geq 99.6\%$) were bought from Sigma Aldrich and used without any further purification. 1-Hexanol (99%, anhydrous) was brought from Acros. Acetone and dichloromethane (DCM) were bought from Biosolve and used without any further purification. Acetonitrile (ACN) HPLC grade was bought from VWR and used without any further purification. Molecular sieves, 3 Å (beads, 8-12 mesh) were purchased from Sigma Aldrich and were activated under vacuum before use.

Synthesis of ZrO_2 nanocrystals with oleate ligands ZrO_2 nanocrystals were synthesized according to Garnweitner *et al.*, using zirconium isopropoxide isopropanol complex (6.6 g, 17 mmol, 1 eq) and benzyl alcohol (60 mL, 580 mmol, 34 eq) at 210 °C for 2 days.⁷⁵ After reaction, a white powder is isolated via centrifugation. The powder is washed three

times with diethyl ether and is then dispersed in 40 mL toluene for functionalizing with 2.4 mL oleic acid (99%). Thus formed nanocrystals are precipitated using 30 mL acetone. Finally, the purified nanocrystals are dispersed in 20 mL of toluene and stored in a fridge. TGA showed the presence of 65% inorganic content and a yield of 43% is obtained.

Synthesis of UiO-66: Synthesis was done with slight modifications to previous reports.^{73,74} ZrCl₄ (3.5 g, 15 mmol) and benzene-1, 4-dicarboxylic acid (2.5 g, 15 mmol) are mixed with 155 mL of dimethyl formamide (DMF) and 1.5 mL of hydrochloric acid (HCl) (37%). The reaction is done in a 1L pressure bottle at 120 °C for 24 hrs. After 24 hours, a white precipitate is formed. The white precipitate is collected via centrifugation. This is washed by adding acetone and shaking for 2 days. The solvent is changed 4 times within the 2 days of washing. The powder is collected using centrifugation at 10000 rpm for 10 min. It was dried in air at 70 °C for 4 h followed by activation at 110 °C for 20 h, and stored in a desiccator.

Synthesis of Zr12 oxo clusters All oxo clusters were synthesized and purified according to our previous report.⁵¹

Catalytic experiments

Ethyl oleate using Zr12 cluster as catalyst. The standard catalytic reaction used 1 mol% of Zr12 cluster as catalyst (0.096 mmol Zr, 64.9 mg cluster). The 1 mol% is calculated with respect to the limiting reagent (carboxylic acid + oleate ligand = 0.8 mmol). The catalyst was transferred to an 8 mL GC vial, together with oleic acid (0.608 mmol, 192 μ L). Furthermore, 4 equivalents of ethanol (3.2 mmol, 186.8 μ L) and 3.6 mL of either *o*-dichlorobenzene (*o*-DBC) or mesitylene is added, together with 100 mg of 3 Å molecular sieves. The total solution is 4 mL and the final oleate/oleic acid concentration is 0.2M. The solution is stirred on a heating block at 120 °C for 12 hrs, after which the yield is determined by ¹H NMR.

Ethyl oleate using 5.6 nm ZrO₂ nanocrystals as catalyst. Oleic acid (0.8 mmol, 252

μL) is mixed with 4 eq of EtOH and 3 Å molecular sieves and made up to 4 mL using o-DCB as the solvent. To this, is added, 0.096 mmol ZrO_2 (18.15 mg) which corresponds to the amount of Zr present in 1 mol% of the **Zr12** cluster. The reaction is stirred in an 8 mL GC vial at 120 °C for 12 hrs, after which the yield is determined by ^1H NMR.

Ethyl oleate using UiO-66 as catalyst. Oleic acid (0.8 mmol, 252 μL) is mixed with 4 eq of EtOH and 3 Å molecular sieves and made up to 4 mL using o-DCB as the solvent. To this, is added, 24.34 mg of MOF UiO-66 (0.096 mmol of Zr). The reaction is stirred in an 8 mL GC vial at 120 °C for 12 hrs, after which the yield is determined by ^1H NMR.

Hexyl oleate using Zr12-oleate as catalyst. 3.8 mmol of oleic acid (1.199 mL) is mixed with 4 eq or 1.2 eq of EtOH and 3 Å molecular sieves. To this, is added, 1 mol% of the Zr12 oleate cluster (405.7 mg)(the total amount of oleic acid and oleate is 5 mmol). The reaction is stirred in an 8 mL GC vial at 120 °C. An aliquot is taken after 3 hrs and 6 hrs and the reaction progress is calculated based on the ^1H NMR data. The catalyst is then recovered by precipitation using acetonitrile and washing with acetone (46%).

Hexyl, 2-Ethylhexyl, benzyl, and neopentyl oleate using Zr12 oleate as catalyst: The reaction is done similarly to the above procedure using 5 mmol of oleic acid and 1.2 equivalent of the respective alcohol.

Hexyl oleate using homogeneous catalysts. 5 mmol of oleic acid (1.578 mL) is mixed with 1.2 eq of hexanol (753.1 μL) and 3 Å molecular sieves (omitted in some reactions). To this, is added, 12 mol% (0.6 mmol) of $\text{Zr}(\text{OPr})_4$, or $\text{Zr}(\text{O}^t\text{Bu})_4$ (233.7 μL), or $\text{Hf}(\text{O}^t\text{Bu})_4$ (242.3 μL), or ZrCl_4 (139.8 mg). The reaction is stirred in a GC vial for 30 min or 3 hrs and analyzed via ^1H NMR. The catalyst is then recovered by precipitation using acetonitrile and washing with acetone.

General instrumentation

The FTIR spectra was done on Perkin Elmer spectrum 2 ATR-FTIR with a diamond crystal. The thermogravimetric analysis (TGA) was performed on a TGA5500 (TA instruments)

instrument. The samples were heated to 900 °C at a ramping rate of 5 °C min⁻¹. At the end an isotherm of 15 min is given to ensure that all the organics are burned out. HR-TEM imaging was carried out in JEOL JEM-F200 operated in the TEM-mode at a beam energy of 200kV.

Nuclear Magnetic Resonance (NMR) Spectroscopy: NMR measurements were recorded at 298 K on Bruker UltraShield 500 spectrometer. In order to track the esterification yield, nuclear magnetic resonance spectroscopy (NMR) was employed as the primary technique. The α proton of the ester formed during oleate esterification shows a distinct peak in the NMR. The integral of this peak was compared with the alkene resonance at 5.4 ppm to determine the percentage conversion. The delay time for the proton NMR was set optimized to reduce the error in the percentage conversion calculation using NMR. A delay time of 10 and 30 seconds shows almost similar results. Therefore the delay time for further studies was fixed at 10 s.

Structural characterization with X-ray total scattering experiments: X-ray total scattering data were collected at beamline 28-ID-2 (XPD) at National Synchrotron Light Source II (NSLS-II), Brookhaven National Laboratory, USA or at beamline P21.1 at PETRA III/DESY in Hamburg, Germany. Measurements were carried out at room temperature on samples prepared in 1 mm polyamide kapton tubes in rapid acquisition mode using a large-area 2D PerkinElmer detector (2048 x 2048 pixels, 200 μm x 200 μm pixel size) with a sample-to-detector distance of 267 mm (28-ID-2) or 350 mm (P21.1). The incident wavelength of the X-rays was $\lambda = 0.1665 \text{ \AA}$ (28-ID-2) and $\lambda = 0.1222 \text{ \AA}$ (P21.1) and the measurement exposure time was 600 s. To calibrate the experimental setup a CeO₂ standard was used while the scattering pattern of pure oleic acid or of the empty kapton was used as background, in accordance with experimental conditions. The data were integrated using pyFAI⁸² and the PDF spectra were obtained using xPDFSuite⁸³ with PDFgetX3 with $Q_{max} = 21.5$, $Q_{min} = 0.8$ and $R_{poly} = 0.99$. The chemical composition of the cluster (Zr₁₂O₆₄C₂₄H₈₀) was used to reduce the data. DiffpyCMI⁸⁴ was used to fit the data by refining scale factor (one per each

phase in case of the dual phase fitting), isotropic atomic displacement parameters (Uiso) and delta2 (coefficient for the 1/r² contribution to peak sharpening).

Acknowledgement

The authors thank the SNF NCCR molecular systems engineering (182895) for funding. T.N.P.V. thanks KU Leuven and Research Foundation Flanders (FWO) for funding. C. Simms thanks the Research Foundation-Flanders (FWO) for the fellowship grant (68090/11C9320N). We thank Jonas Zurflüh for helping us with the analysis. This research used resources of beamline 28-ID-2 of the National Synchrotron Light Source II, a U.S. Department of Energy (DOE) Office of Science User Facility operated for the DOE Office of Science by Brookhaven National Laboratory under Contract No. DE-SC0012704. We would like to thank Dr. Sanjit K. Ghose and Dr. Hui Zhong for their assistance in using the beamline for PDF acquisition. Beamtime was allocated for proposal number 313157. We also acknowledge DESY (Hamburg, Germany), a member of the Helmholtz Association HGF, for the provision of experimental facilities. Parts of this research were carried out using beamline P21.1 at DESY and we would like to thank Dr. Ann-Christin Dippel, Dr. Jiatu Liu and Dr. Fernando Igoa for assistance in using the beamline for PDF acquisition (proposal I-20231114 EC). We also thank Prof. Dr. Konrad Tiefenbacher, Prof. Dr. Francisco De Azambuja, and Dr. Evert Dhaene for all the fruitful discussions.

Supporting Information Available

Characterization of the catalysts used, optimization of esterification, calculation of turnover number, PDF refinements are available in the supporting information.

References

- (1) Murray, C.; Norris, D. J.; Bawendi, M. G. Synthesis and characterization of nearly monodisperse CdE (E= sulfur, selenium, tellurium) semiconductor nanocrystallites. *Journal of the American Chemical Society* **1993**, *115*, 8706–8715.
- (2) Liu, Y.; Zhao, G.; Wang, D.; Li, Y. Heterogeneous catalysis for green chemistry based on nanocrystals. *National Science Review* **2015**, *2*, 150–166.
- (3) Choudary, B. M.; Mulukutla, R. S.; Klabunde, K. J. Benzylolation of Aromatic Compounds with Different Crystallites of MgO. *Journal of the American Chemical Society* **2003**, *125*, 2020–2021, PMID: 12590509.
- (4) Colloidal nanocrystals for heterogeneous catalysis. *Nano Today* **2019**, *24*, 15–47.
- (5) Stracke, J. J.; Finke, R. G. Electrocatalytic water oxidation beginning with the cobalt polyoxometalate [Co₄ (H₂O)₂ (PW₉O₃₄)₂]¹⁰⁻: identification of heterogeneous CoO_x as the dominant catalyst. *Journal of the American Chemical Society* **2011**, *133*, 14872–14875.
- (6) Van den Eynden, D.; Pokratath, R.; De Roo, J. Nonaqueous Chemistry of Group 4 Oxo Clusters and Colloidal Metal Oxide Nanocrystals. *Chemical Reviews* **2022**, *122*, 10538–10572.
- (7) Zhang, Y.; De Azambuja, F.; Parac-Vogt, T. N. The forgotten chemistry of group (IV) metals: A survey on the synthesis, structure, and properties of discrete Zr (IV), Hf (IV), and Ti (IV) oxo clusters. *Coordination Chemistry Reviews* **2021**, *438*, 213886.
- (8) Valenzano, L.; Civalieri, B.; Chavan, S.; Bordiga, S.; Nilsen, M. H.; Jakobsen, S.; Lillerud, K. P.; Lamberti, C. Disclosing the complex structure of UiO-66 metal organic framework: a synergic combination of experiment and theory. *Chemistry of Materials* **2011**, *23*, 1700–1718.

- (9) Hennig, C.; Weiss, S.; Kraus, W.; Kretzschmar, J.; Scheinost, A. C. Solution species and crystal structure of Zr (IV) acetate. *Inorganic chemistry* **2017**, *56*, 2473–2480.
- (10) Cargnello, M.; Doan-Nguyen, V. V. T.; Gordon, T. R.; Diaz, R. E.; Stach, E. A.; Gorte, R. J.; Fornasiero, P.; Murray, C. B. Control of Metal Nanocrystal Size Reveals Metal-Support Interface Role for Ceria Catalysts. *Science* **2013**, *341*, 771–773.
- (11) Lee, I.; Morales, R.; Albiter, M. A.; Zaera, F. Synthesis of heterogeneous catalysts with well shaped platinum particles to control reaction selectivity. *Proceedings of the National Academy of Sciences* **2008**, *105*, 15241–15246.
- (12) Goodman, E. D.; Dai, S.; Yang, A.-C.; Wrasman, C. J.; Gallo, A.; Bare, S. R.; Hoffman, A. S.; Jaramillo, T. F.; Graham, G. W.; Pan, X.; Cargnello, M. Uniform Pt/Pd Bimetallic Nanocrystals Demonstrate Platinum Effect on Palladium Methane Combustion Activity and Stability. *ACS Catalysis* **2017**, *7*, 4372–4380.
- (13) Markovic, N. M.; Gasteiger, H. A.; Ross Jr, P. N. Oxygen reduction on platinum low-index single-crystal surfaces in sulfuric acid solution: rotating ring-Pt (hkl) disk studies. *The Journal of Physical Chemistry* **1995**, *99*, 3411–3415.
- (14) Yamamoto, K.; Imaoka, T.; Chun, W.-J.; Enoki, O.; Katoh, H.; Takenaga, M.; Sonoi, A. Size-specific catalytic activity of platinum clusters enhances oxygen reduction reactions. *Nature chemistry* **2009**, *1*, 397–402.
- (15) Ng, J. W. D.; Hellstern, T. R.; Kibsgaard, J.; Hinckley, A. C.; Benck, J. D.; Jaramillo, T. F. Polymer electrolyte membrane electrolyzers utilizing non-precious Mo-based hydrogen evolution catalysts. *ChemSusChem* **2015**, *8*, 3512–3519.
- (16) Subramanian, V.; Wolf, E. E.; Kamat, P. V. Catalysis with TiO₂/gold nanocomposites. Effect of metal particle size on the Fermi level equilibration. *Journal of the American Chemical Society* **2004**, *126*, 4943–4950.

- (17) Gordon, T. R.; Cargnello, M.; Paik, T.; Mangolini, F.; Weber, R. T.; Fornasiero, P.; Murray, C. B. Nonaqueous synthesis of TiO₂ nanocrystals using TiF₄ to engineer morphology, oxygen vacancy concentration, and photocatalytic activity. *Journal of the American Chemical Society* **2012**, *134*, 6751–6761.
- (18) Chen, S.; Takata, T.; Domen, K. Particulate photocatalysts for overall water splitting. *Nature Reviews Materials* **2017**, *2*, 1–17.
- (19) Astruc, D.; Lu, F.; Aranzaes, J. R. Nanoparticles as recyclable catalysts: the frontier between homogeneous and heterogeneous catalysis. *Angewandte Chemie International Edition* **2005**, *44*, 7852–7872.
- (20) Xia, C.; Wu, J.; Delbari, S. A.; Namini, A. S.; Yuan, Y.; Van Le, Q.; Kim, D.; Varma, R. S.; Ali, T.; Jang, H. W., et al. Metal-organic framework-based nanostructured catalysts: Applications in efficient organic transformations. *Molecular Catalysis* **2023**, *546*, 113217.
- (21) Chughtai, A. H.; Ahmad, N.; Younus, H. A.; Laypkov, A.; Verpoort, F. Metal-organic frameworks: versatile heterogeneous catalysts for efficient catalytic organic transformations. *Chemical Society Reviews* **2015**, *44*, 6804–6849.
- (22) Bavykina, A.; Kolobov, N.; Khan, I. S.; Bau, J. A.; Ramirez, A.; Gascon, J. Metal-organic frameworks in heterogeneous catalysis: recent progress, new trends, and future perspectives. *Chemical reviews* **2020**, *120*, 8468–8535.
- (23) Panda, J.; Sahoo, T.; Swain, J.; Panda, P. K.; Tripathy, B. C.; Samantaray, R.; Sahu, R. The Journey from Porous Materials to Metal-organic Frameworks and their Catalytic Applications: A Review. *Current Organic Synthesis* **2023**, *20*, 220–237.
- (24) Andrade, L. S.; Lima, H. H.; Silva, C. T.; Amorim, W. L.; Poco, J. G.; Lopez-Castillo, A.; Kirillova, M. V.; Carvalho, W. A.; Kirillov, A. M.; Mandelli, D. Metal-

- organic frameworks as catalysts and biocatalysts for methane oxidation: The current state of the art. *Coordination Chemistry Reviews* **2023**, *481*, 215042.
- (25) Dong, H.; Zhu, H.; Li, Q.; Zhou, M.; Ren, X.; Ma, T.; Liu, J.; Zeng, Z.; Luo, X.; Li, S., et al. Atomically Structured Metal-Organic Frameworks: A Powerful Chemical Path for Noble Metal-Based Electrocatalysts. *Advanced Functional Materials* **2023**, 2300294.
- (26) Li, Y.; Wu, Y.; Liu, K.; Delbari, S. A.; Kim, A.; Namini, A. S.; Van Le, Q.; Shokouhimehr, M.; Xia, C.; Jang, H. W., et al. Metal-organic framework-based nanostructured catalysts: Applications in biomass conversion. *Fuel* **2023**, *340*, 127482.
- (27) KACEM, M.; Mustapha, D. An overview of the progress of MOFs-based hybrid materials as efficient catalysts for Knoevenagel condensation. *Inorganic Chemistry Communications* **2023**, 111561.
- (28) Zhou, H.-C.; Long, J. R.; Yaghi, O. M. Introduction to metal-organic frameworks. 2012.
- (29) Razavi, S. A. A.; Morsali, A. Linker functionalized metal-organic frameworks. *Coordination Chemistry Reviews* **2019**, *399*, 213023.
- (30) Zhang, Y.; Yang, X.; Zhou, H.-C. Synthesis of MOFs for heterogeneous catalysis via linker design. *Polyhedron* **2018**, *154*, 189–201.
- (31) Lu, W.; Wei, Z.; Gu, Z.-Y.; Liu, T.-F.; Park, J.; Park, J.; Tian, J.; Zhang, M.; Zhang, Q.; Gentle III, T., et al. Tuning the structure and function of metal-organic frameworks via linker design. *Chemical Society Reviews* **2014**, *43*, 5561–5593.
- (32) Yuan, S.; Qin, J.-S.; Lollar, C. T.; Zhou, H.-C. Stable metal-organic frameworks with group 4 metals: current status and trends. *ACS central science* **2018**, *4*, 440–450.
- (33) Feng, L.; Pang, J.; She, P.; Li, J.-L.; Qin, J.-S.; Du, D.-Y.; Zhou, H.-C. Metal-organic frameworks based on group 3 and 4 metals. *Advanced Materials* **2020**, *32*, 2004414.

- (34) Dissegna, S.; Epp, K.; Heinz, W. R.; Kieslich, G.; Fischer, R. A. Defective metal-organic frameworks. *Advanced Materials* **2018**, *30*, 1704501.
- (35) Lu, Z.; Liu, J.; Zhang, X.; Liao, Y.; Wang, R.; Zhang, K.; Lyu, J.; Farha, O. K.; Hupp, J. T. Node-accessible zirconium MOFs. *Journal of the American Chemical Society* **2020**, *142*, 21110–21121.
- (36) Dai, S.; Simms, C.; Dovgaliuk, I.; Patriarche, G.; Tissot, A.; Parac-Vogt, T. N.; Serre, C. Monodispersed MOF-808 nanocrystals synthesized via a scalable room-temperature approach for efficient heterogeneous peptide bond hydrolysis. *Chemistry of Materials* **2021**, *33*, 7057–7066.
- (37) Villoria-del Álamo, B.; Rojas-Buzo, S.; García-García, P.; Corma, A. Zr-MOF-808 as Catalyst for Amide Esterification. *Chemistry—A European Journal* **2021**, *27*, 4588–4598.
- (38) Cirujano, F.; Corma, A.; i Xamena, F. L. Zirconium-containing metal organic frameworks as solid acid catalysts for the esterification of free fatty acids: Synthesis of biodiesel and other compounds of interest. *Catalysis Today* **2015**, *257*, 213–220.
- (39) de Azambuja, F.; Loosen, A.; Conic, D.; van den Besselaar, M.; Harvey, J. N.; Parac-Vogt, T. N. En route to a heterogeneous catalytic direct peptide bond formation by Zr-based metal–organic framework catalysts. *Acs Catalysis* **2021**, *11*, 7647–7658.
- (40) Nguyen, L. H. T.; Nguyen, T. T. T.; Dang, Y. T.; Tran, P. H.; Le Hoang Doan, T. Microwave-Assisted Synthesis as an Efficient Method to Enhance the Catalytic Activity of Zr-Based Metal Organic Framework UiO-66 in a Heterocyclization Reaction. *Asian Journal of Organic Chemistry* **2019**, *8*, 2276–2281.
- (41) Gong, W.; Chen, X.; Jiang, H.; Chu, D.; Cui, Y.; Liu, Y. Highly stable Zr (IV)-based metal–organic frameworks with chiral phosphoric acids for catalytic asymmetric tandem reactions. *Journal of the American Chemical Society* **2019**, *141*, 7498–7508.

- (42) Ghobakhloo, F.; Azarifar, D.; Mohammadi, M.; Keypour, H.; Zeynali, H. Copper (II) Schiff-base complex modified UiO-66-NH₂ (Zr) metal–organic framework catalysts for Knoevenagel condensation–Michael addition–cyclization reactions. *Inorganic Chemistry* **2022**, *61*, 4825–4841.
- (43) Rimoldi, M.; Howarth, A. J.; DeStefano, M. R.; Lin, L.; Goswami, S.; Li, P.; Hupp, J. T.; Farha, O. K. Catalytic zirconium/hafnium-based metal–organic frameworks. *Acs Catalysis* **2017**, *7*, 997–1014.
- (44) Loosen, A.; de Azambuja, F.; Smolders, S.; Moons, J.; Simms, C.; De Vos, D.; Parac-Vogt, T. N. Interplay between structural parameters and reactivity of Zr₆-based MOFs as artificial proteases. *Chemical Science* **2020**, *11*, 6662–6669.
- (45) Tuttle, R. R.; Folkman, S. J.; Rubin, H. N.; Finke, R. G.; Reynolds, M. M. Copper Metal–Organic Framework Surface Catalysis: Catalyst Poisoning, IR Spectroscopic, and Kinetic Evidence Addressing the Nature and Number of the Catalytically Active Sites En Route to Improved Applications. *ACS Applied Materials & Interfaces* **2020**, *12*, 39043–39055.
- (46) Semrau, A. L.; Stanley, P. M.; Urstoeger, A.; Schuster, M.; Cokoja, M.; Fischer, R. A. Substantial Turnover Frequency Enhancement of MOF Catalysts by Crystallite Downsizing Combined with Surface Anchoring. *ACS Catalysis* **2020**, *10*, 3203–3211.
- (47) Feng, D.; Gu, Z.-Y.; Li, J.-R.; Jiang, H.-L.; Wei, Z.; Zhou, H.-C. Zirconium-Metalloporphyrin PCN-222: Mesoporous Metal–Organic Frameworks with Ultrahigh Stability as Biomimetic Catalysts. *Angewandte Chemie: International Edition* **2012**, *51*, 10307–10310.
- (48) Li, P.; Klet, R. C.; Moon, S.-Y.; Wang, T. C.; Deria, P.; Peters, A. W.; Klahr, B. M.; Park, H.-J.; Al-Juaid, S. S.; Hupp, J. T.; Farha, O. K. Synthesis of nanocrystals of

- Zr-based metal–organic frameworks with csq-net: significant enhancement in the degradation of a nerve agent simulant. *Chemical Communications* **2015**, *51*, 10925–10928.
- (49) Li, P.; Moon, S.-Y.; Guelta, M. A.; Lin, L.; Gómez-Gualdrón, D. A.; Snurr, R. Q.; Harvey, S. P.; Hupp, J. T.; Farha, O. K. Nanosizing a Metal–Organic Framework Enzyme Carrier for Accelerating Nerve Agent Hydrolysis. *ACS Nano* **2016**, *10*, 9174–9182.
- (50) Majewski, M. B.; Noh, H.; Islamoglu, T.; Farha, O. K. NanoMOFs: little crystallites for substantial applications. *Journal of Materials Chemistry A* **2018**, *6*, 7338–7350.
- (51) Van den Eynden, D.; Pokratath, R.; Mathew, J. P.; Goossens, E.; De Buysser, K.; De Roo, J. Fatty acid capped, metal oxo clusters as the smallest conceivable nanocrystal prototypes. *Chem. Sci.* **2023**, *14*, 573–585.
- (52) Cao, Y.; Chen, Q.; Shen, C.; He, L. Polyoxometalate-based catalysts for CO₂ conversion. *Molecules* **2019**, *24*, 2069.
- (53) Wang, S.-S.; Yang, G.-Y. Recent advances in polyoxometalate-catalyzed reactions. *Chemical reviews* **2015**, *115*, 4893–4962.
- (54) Kamata, K.; Sugahara, K. Base catalysis by mono-and polyoxometalates. *Catalysts* **2017**, *7*, 345.
- (55) Zhang, Y.; De Azambuja, F.; Parac-Vogt, T. N. Zirconium oxo clusters as discrete molecular catalysts for the direct amide bond formation. *Catalysis Science & Technology* **2022**, *12*, 3190–3201.
- (56) Sun, S.-N.; Niu, Q.; Lin, J.-M.; He, L.-L.; Shi, J.-W.; Huang, Q.; Liu, J.; Lan, Y.-Q. Sulfur atom-directed metal–ligand synergistic catalysis in zirconium/hafnium-oxo clusters for highly efficient amine oxidation. *Science Bulletin* **2023**,

- (57) Faccioli, F.; Bauer, M.; Pedron, D.; Sorarù, A.; Carraro, M.; Gross, S. Hydrolytic Stability and Hydrogen Peroxide Activation of Zirconium-Based Oxoclusters. *European Journal of Inorganic Chemistry* **2015**, *2015*, 210–225.
- (58) Moons, J.; de Azambuja, F.; Mihailovic, J.; Kozma, K.; Smiljanic, K.; Amiri, M.; Cirkovic Velickovic, T.; Nyman, M.; Parac-Vogt, T. N. Discrete Hf₁₈ Metal-oxo Cluster as a Heterogeneous Nanozyme for Site-Specific Proteolysis. *Angewandte Chemie International Edition* **2020**, *59*, 9094–9101.
- (59) Stacy, C. J.; Melick, C. A.; Cairncross, R. A. Esterification of free fatty acids to fatty acid alkyl esters in a bubble column reactor for use as biodiesel. *Fuel processing technology* **2014**, *124*, 70–77.
- (60) Knothe, G.; Razon, L. F. Biodiesel fuels. *Progress in Energy and Combustion Science* **2017**, *58*, 36–59.
- (61) Yaakob, Z.; Narayanan, B. N.; Padikkaparambil, S., et al. A review on the oxidation stability of biodiesel. *Renewable and Sustainable Energy Reviews* **2014**, *35*, 136–153.
- (62) da Silva, M. V.; Souza, A. B.; de Castro, H. F.; Aguiar, L. G.; de Oliveira, P. C.; de Freitas, L. Synthesis of 2-ethylhexyl oleate catalyzed by *Candida antarctica* lipase immobilized on a magnetic polymer support in continuous flow. *Bioprocess and biosystems engineering* **2020**, *43*, 615–623.
- (63) Hosney, H.; Mustafa, A. Semi-continuous production of 2-ethyl hexyl ester in a packed bed reactor: optimization and economic evaluation. *Journal of oleo science* **2020**, *69*, 31–41.
- (64) de Oliveira, D. P.; do Valle Moreira, T.; Batista, N. V.; de Souza Filho, J. D.; Amaral, F. A.; Teixeira, M. M.; de Pádua, R. M.; Braga, F. C. Esterification of trans-aconitic acid improves its anti-inflammatory activity in LPS-induced acute arthritis. *Biomedicine Pharmacotherapy* **2018**, *99*, 87–95.

- (65) Ting, R. R.; Agapay, R.; Angkawijaya, A. E.; Tran Nguyen, P. L.; Truong, C. T.; Ju, Y.-H. Diglyceride production via noncatalyzed esterification of glycerol and oleic acid. *Asia-Pacific Journal of Chemical Engineering* **2019**, *14*, e2383, e2383 APJ-19-0193.R1.
- (66) Krishna, S. H.; Karanth, N. G. LIPASES AND LIPASE-CATALYZED ESTERIFICATION REACTIONS IN NONAQUEOUS MEDIA. *Catalysis Reviews* **2002**, *44*, 499–591.
- (67) Che Marzuki, N. H.; Mahat, N. A.; Huyop, F.; Aboul-Enein, H. Y.; Wahab, R. A. Sustainable production of the emulsifier methyl oleate by *Candida rugosa* lipase nanoconjugates. *Food and Bioproducts Processing* **2015**, *96*, 211–220.
- (68) Yuan, B.; Wang, Y.; Wang, M.; Gou, G.; Li, L. Metalorganic frameworks as recyclable catalysts for efficient esterification to synthesize traditional plasticizers. *Applied Catalysis A: General* **2021**, *622*, 118212.
- (69) V. Punsuvon, P. S. M. T., R. Nokkaew; Karnasuta, S. The Optimization of Esterification Reaction for Biodiesel Production from Animal Fat. *Energy Sources, Part A: Recovery, Utilization, and Environmental Effects* **2015**, *37*, 846–853.
- (70) Patel, A.; Narkhede, N. 12-Tungstophosphoric Acid Anchored to Zeolite H: Synthesis, Characterization, and Biodiesel Production by Esterification of Oleic Acid with Methanol. *Energy & Fuels* **2012**, *26*, 6025–6032.
- (71) Di Serio, M.; Tesser, R.; Pengmei, L.; Santacesaria, E. Heterogeneous Catalysts for Biodiesel Production. *Energy & Fuels* **2008**, *22*, 207–217.
- (72) Wang, H.; Covarrubias, J.; Prock, H.; Wu, X.; Wang, D.; Bossmann, S. H. Acid-Functionalized Magnetic Nanoparticle as Heterogeneous Catalysts for Biodiesel Synthesis. *The Journal of Physical Chemistry C* **2015**, *119*, 26020–26028.

- (73) Vermoortele, F.; Bueken, B.; Le Bars, G.; Van de Voorde, B.; Vandichel, M.; Houthoofd, K.; Vimont, A.; Daturi, M.; Waroquier, M.; Van Speybroeck, V., et al. Synthesis modulation as a tool to increase the catalytic activity of metal–organic frameworks: the unique case of UiO-66 (Zr). *Journal of the American Chemical Society* **2013**, *135*, 11465–11468.
- (74) Ly, H. G. T.; Fu, G.; de Azambuja, F.; De Vos, D.; Parac-Vogt, T. N. Nanozymatic activity of UiO-66 metal–organic frameworks: tuning the nanopore environment enhances hydrolytic activity toward peptide bonds. *ACS Applied Nano Materials* **2020**, *3*, 8931–8938.
- (75) Garnweitner, G.; Goldenberg, L.; Sakhno, O.; Antonietti, M.; Niederberger, M.; Stumpe, J. Large-Scale Synthesis of Organophilic Zirconia Nanoparticles and their Application in Organic–Inorganic Nanocomposites for Efficient Volume Holography. *Small* **2007**, *3*, 1626–1632.
- (76) De Roo, J.; Van Driessche, I.; Martins, J. C.; Hens, Z. Colloidal metal oxide nanocrystal catalysis by sustained chemically driven ligand displacement. *Nature Materials* **2016**, *15*, 517–521.
- (77) De Roo, J.; Yazdani, N.; Drijvers, E.; Lauria, A.; Maes, J.; Owen, J. S.; Van Driessche, I.; Niederberger, M.; Wood, V.; Martins, J. C.; Infante, I.; Hens, Z. Probing Solvent–Ligand Interactions in Colloidal Nanocrystals by the NMR Line Broadening. *Chemistry of Materials* *30*, 5485–5492.
- (78) De Roo, J. The Surface Chemistry of Colloidal Nanocrystals Capped by Organic Ligands. *Chemistry of Materials* *35*, 3781–3792.
- (79) Puchberger, M.; Kogler, F. R.; Jupa, M.; Gross, S.; Fric, H.; Kickelbick, G.; Schubert, U. Can the clusters $[\text{Zr}_6\text{O}_4(\text{OH})_4(\text{OOCR})_{12}]$ and $[\text{Zr}_6\text{O}_4(\text{OH})_4(\text{OOCR})_{12}]_2$ be converted into each other? 2006.

- (80) Ishihara, K.; Ohara, S.; Yamamoto, H. Direct Condensation of Carboxylic Acids with Alcohols Catalyzed by Hafnium(IV) Salts. *Science* **2000**, *290*, 1140–1142.
- (81) Dhaene, E.; Seno, C.; De Roo, J. Synthesis of Zirconium (IV) and Hafnium (IV) isopropoxide and tert-butoxide. **2023**,
- (82) Ashiotis, G.; Deschildre, A.; Nawaz, Z.; Wright, J. P.; Karkoulis, D.; Picca, F. E.; Kieffer, J. The fast azimuthal integration Python library: pyFAI. *Journal of applied crystallography* **2015**, *48*, 510–519.
- (83) Yang, X.; Juhas, P.; Farrow, C. L.; Billinge, S. J. xPDFsuite: an end-to-end software solution for high throughput pair distribution function transformation, visualization and analysis. *arXiv preprint arXiv:1402.3163* **2014**,
- (84) Juhás, P.; Farrow, C.; Yang, X.; Knox, K.; Billinge, S. Complex modeling: a strategy and software program for combining multiple information sources to solve ill posed structure and nanostructure inverse problems. *Acta Crystallographica Section A: Foundations and Advances* **2015**, *71*, 562–568.